The Development of CO_2 Plume in CO_2 Sequestration in the Aquifer

Hao Fu[1], Yifu Long[2], Sai Wang[1], Yanbo Wang[1], Peng Yu[3] and Kegang Ling[1], (1) University of North Dakota, Grand Forks, ND, USA, (2) Missouri University of Science and Technology, Rolla, MO, USA, (3) Beibu Gulf University, Qinzhou, Guangxi, China

Abstract

Geological carbon sequestration through injecting large-scale carbon dioxide (CO_2) into the deep saline aquifers represents a long-term storage of CO_2. In the CO_2 sequestration process, the injected CO_2 is displacing water from the injection point and is expected to remain in the reservoir. Due to the nature of one phase displacing another phase in porous media, it is noted that different water saturation exists in the CO_2 plume during the displacement. Water distribution in the plume will affect the size of the plume subsurface. Furthermore, the gravitational segregation between CO_2 and water will cause overriding-tonguing during the injection and impact the shape of plume. To better understand the CO_2 movement underground and development of CO_2 plume, it is necessary to take the two-phase flow and gravity force effects into account when evaluating CO_2 displacing water. The displacement of water by injecting CO_2 is not a piston-like process in aquifer. Because water is the wetting phase and CO_2 is the non-wetting phase when two phases flow in reservoir, water occupies the surface of matrix and small pores while CO_2 resides in large pores and centers of pores. As a result, various water saturations distribute behind CO_2 front during the displacement. The distribution is a function of fluid and rock properties, fluid-rock interaction, and injection operation. In this study, these factors are considered when developing new models to predict CO_2 plume evolution during injection. Mass conservation, multiphase flow, and equation-of-states are applied in the derivation of the models, which guarantees a rigorous approach in the investigation. The modeling results indicate that CO_2 does not displace water completely away from the plume. The shape of the CO_2 front is controlled by the relative permeability of two phases and capillary pressure. Water saturation profile from CO_2 injecting point to the displacement front shows that water saturation behind the CO_2 front increases outwardly, and the change in saturation is non-linear. The injection rate impacts the sharpness of the CO_2 front, thus leads to different gas plume sizes for same injection volume. The outward movement of the CO_2 front decelerates as injection time goes on. The research illustrates that injection experiences two stages: transient and steady-state, in which the displacement behavior and the development of gas plume vary. Although the duration of transient stage is dictated by size of aquifer and is relatively short comparing with steady-state stage, its influence on the development of CO_2 plume cannot be neglected when selecting gas compressor horsepower and determining injection rate.

Introduction

Greenhouse effect is one of the processes that cause the arguable global warming in recent years. When the energy from the Sun reaches the Earth, part of it is reflected back to the space while the rest is absorbed and reradiated by the Earth's atmosphere, which consists of greenhouse gases. CO_2 is one of the greenhouse gases that contribute to the trapping of heat that radiates from Earth. Greenhouse gases in the Earth's atmosphere are mainly CO_2, methane, nitrous oxide, hydrofluorocarbons, sulfur hexafluoride, fluorinated gases, ozone (O_3), and water vapor, etc. Table 1 (Haynes, 2016) shows the concentration of different gas in atmosphere. It is noted that the contribution of each greenhouse gas to the absorption of

heat depends on its concentration and its global warming potential (GWP). GWP is used to reflect how long a greenhouse gas remains in the atmosphere, on average, and how strongly it absorbs energy. Gases with a higher GWP absorb more energy, per pound, than gases with a lower GWP, and thus contribute more to warming Earth. GWP of greenhouse gases is listed in Table 2 (U.S. EPA, 2019). Although the global warming potential of CO_2 is not the highest, its effect on global warming is significant due to the relatively high concentration and the increasing emission volume during last several decades. Many researches indicate that anthropogenic greenhouse gases emitting to the atmosphere are the main cause of global warming. Fig. 1 illustrates that the emission of CO_2 has increased dramatically since industrial revolution (Ritchie and Roser, 2019). Fig. 2 is the corresponding change of CO_2 concentration in atmosphere as a result of increase in CO_2 emission. CO_2 emission is from burning fossil fuels, solid waste, trees and other biological materials. Chemical reactions also emit CO_2.

Table 1. Major constituents of dry air, by volume (Haynes, 2016)

Gas		**Volume[A]**	
Name	Formula	in ppmv[B]	mole %
Nitrogen	N_2	780,840	78.084
Oxygen	O_2	209,460	20.946
Argon	Ar	9,340	0.9340
Carbon dioxide	CO_2	413.32	0.041332
Neon	Ne	18.18	0.001818
Helium	He	5.24	0.000524
Methane	CH_4	1.87	0.000187
Krypton	Kr	1.14	0.000114
Not included in above dry atmosphere:			
Water vapor[C]	H_2O	0–30,000[D]	0–3%[D]

notes:
[A] Volume fraction is equal to mole fraction for ideal gas only,
[B] ppmv: parts per million by volume
[C] Water vapor is about 0.25% *by mass* over full atmosphere
[D] Water vapor strongly varies locally (Wallace et al., 2006)

Table 2. Global Warming Potentials and Atmospheric Lifetimes (U.S. EPA, 2019)

Gas	**Atmospheric Lifetime (years)**	**GWP[a]**
Carbon dioxide (CO_2)	50-200	1
Methane (CH_4)[b]	12±3	21
Nitrous oxide (N_2O)	120	310
HFC-23	264	11,700
HFC-32	5.6	650

HFC-125	32.6	2,800
HFC-134a	14.6	1,300
HFC-143a	48.3	3,800
HFC-152a	1.5	140
HFC-227ea	36.5	2,900
HFC-236fa	209	6,300
HFC-4310mee	17.1	1,300
CF_4	50,000	6,500
C_2F_6	10,000	9,200
C_4F_{10}	2,600	7,000
C_6F_{14}	3,200	7,400
SF_6	3,200	23,900

[a] 100 year time horizon

[b] The methane GWP includes the direct effects and those indirect effects due to the production of tropospheric ozone and stratospheric water vapor. The indirect effect due to the production of CO_2 is not included.

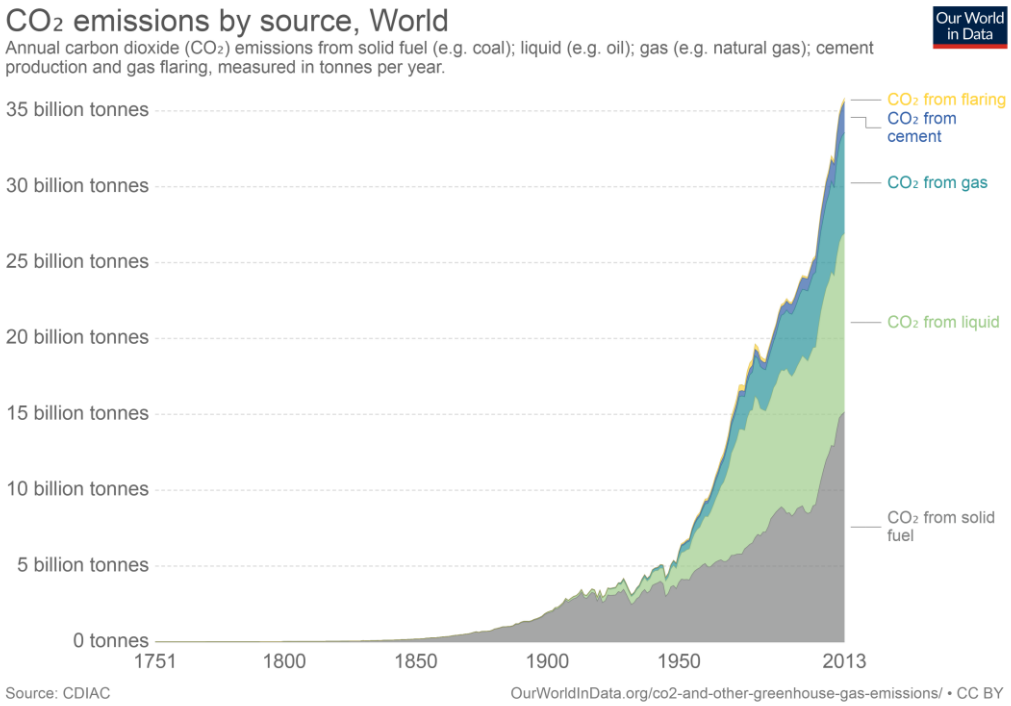

Figure 1. Global emission of CO_2 has increased significantly since industrial evolution (Ritchie and Roser, 2019)

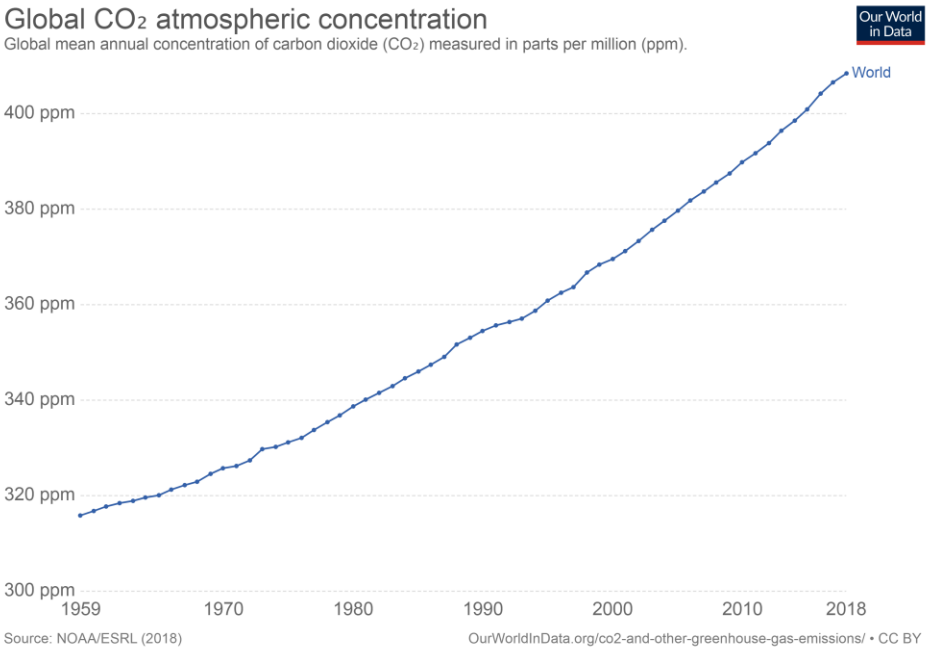

Figure 2. The change of CO_2 concentration in atmosphere (Ritchie and Roser, 2019)

CO_2 can be removed from the atmosphere by the biological carbon cycle, or the photosynthesis, a process by which green plants and some organisms use sunlight to synthesize foods from CO_2 and water. Unfortunately, the amount of CO_2 can be consumed by photosynthesis is lagged behind the CO_2 emission as global population increases. To reduce the concentration of CO_2 in atmosphere and alleviate the global warming, two approaches are employed. One is to reduce the emission of CO_2 through improving fuel efficiency, moving to clean energy or renewable energy such as wind, solar, replacing coal/oil with less carbon-intense fuel (natural gas). Another is the sequestration of CO_2. It is a long-term storage of CO_2 to slow the atmosphere and marine accumulation of CO_2 to mitigate global warming. In the sequestration, CO_2 is captured through biological, chemical, and physical process and then transported and stored in subsurface aquifers, coal beds, depleted oil and gas reservoirs, and ocean water. The storage of CO_2 underground in aquifers, coal beds, depleted oil and gas reservoirs is often referred to geological sequestration.

When selecting a site for geological sequestration, several parameters are considered: reservoir porosity, permeability, existing of fault, sealability of caprock, geometry of reservoir, formation depth, and formation thickness. Porosity and thickness affect the formation storage capacity. Permeability dictates the injection rate and migration of CO_2 in formation. Faults cause the non-uniform flow or tonging phenomenon. Faults in the reservoir are the preferential path for CO_2 to flow. Caprock keeps CO_2 remaining in formation for a long geological time after the injection. Once injected, the CO_2 plume will rise via buoyant forces, since it is less dense than oil and water. Once it encounters a caprock, it will spread laterally until it encounters a gap. If there are fault planes in caprock, there is a possibility the CO_2 could migrate along the fault to the surface. Reservoir geometry controls the distribution and migration direction of CO_2. Formation depth is related to pore pressure, thus impacts the storage capacity and power to inject CO_2.

Numerous researches have been focusing on the storage site selection, dynamics of CO_2 injection and storage in formation, CO_2 migration in reservoir, and possible CO_2 leak through caprock. House et al.

(2003) simulated CO_2 sequestration in two gas fields in North Sea. The gas reservoirs contain 4-9% CO_2 are high permeability sandstone. The authors created two models to estimate the ultimate storage capacity of the reservoir and assess the risk of reservoir leakage. One model assumed a homogeneous sand with properties of the Utsira sand in the Sleipner area. Another based on a hypothetical faulted anticline with high vertical permeability to fault. The results indicated that geologic complexity is a factor influencing migration of CO_2 in the Miocene reservoir sand and the high vertical permeability faults provide high permeability conduits for the CO_2 leak out of the sequestration reservoir. Akanni et al. (2004) developed material balance model for CO_2 sequestration in depleted gas reservoirs. The storage of CO_2 in dry gas, wet gas, and gas condensate reservoir is compared with depleted oil reservoir. The models calculated higher CO_2 storage volume in gas reservoir than oil reservoir and resulted in higher gas recovery than oil recovery. The developed material balance equations can be utilized to predict CO_2 sequestration volume and survey sequestration operation during injection. p/z plot to forecast the sequestration were also presented. Izgec et al. (2005) used experiment and numerical simulation to investigate the injection of CO_2 in deep saline aquifer. The target formation is Midyat carbonate aquifer located in south-east Turkey. Computerized tomography (CT) was used to monitor porosity and permeability change at different CO_2 injection rates, pressures, and temperatures. The effect of salt concentration on the rock property change was also investigated. The experiment was used to calibrate numerical model created by a finite difference, non-isothermal compositional simulator. Solution and dissolution of carbonates via chemical reaction were considered. Bennion and Bachu (2005) presented the relative permeability of three sandstone and three carbonate formation in the Wabamun Lake area southwest of Edmonton in Alberta, Canada, where four coal-fired power plants which produce large volume of CO_2 are located. The formations are representative of the in-situ temperature, pressure, salinity, porosity and permeability characteristics of deep saline aquifers in on-shore North American sedimentary basins. The impact of CO_2-water relative permeability on the CO_2 displacing water performance during the CO_2 injection and on ultimate storage capacity was studied. Spiteri et al. (2005) investigated the hysteresis in the relative permeability of the hydrocarbon phase in a two-phase system. The hysteresis is then evaluated to model geological CO_2 sequestration in saline aquifers. In the sequestration, CO_2 is the non-wetting phase and the trapping of the CO_2 is an essential mechanism during lateral and upward migration of CO_2 plume. Sakurai et al. (2006) described the monitoring of saturation change in a CO_2 sequestration in a pilot test in South Lib erty field, Dayton, Texas. The monitoring was through an observation well that was 100 ft away from the injection well. The depth of the target aquifer is 5000 ft with porosity of 32-35% and air permeability of 2500 mD. 1600 metric tons of CO_2 was injected for eleven days. Because of high formation water salinity, along with high porosity, a pulsed neutron tool was selected as the primary log for monitoring saturation changes through change of thermal neutron absorption cross-section. The C/O ratio measurement and dipole acoustic tool were also used to estimate saturation changes. Breakthrough of CO_2 was observed on the third day. At the end of the injection phase, CO_2 saturation of up to 80% was accounted in the observation well. Even four and a half months after the injection experiments, CO_2 saturation of up to 40% was found in the vicinity of the observation and the injection wells, along with temperature anomalies. Schembre-McCabe et al. (2007) researched the mechanistic of CO_2 sequestration in aquifer and depleted hydrocarbon reservoirs using a compositional simulator. The effects of relative permeability and mobility of different phase, damage due to geochemical reaction, stimulation, and nearby injectors were probed. Their study showed that due to limited storage capacity of a reservoir, injectivity declines during the injection stage. This has impact on injector number. Interference among injectors also affects injector performance. Riaz and Tchelepi (2008) analyzed major factors that control the distribution of CO_2 plume by considering the buoyancy and ignoring trapping, dissolution and chemical reaction. One-dimensional model was applied to characterize a pair of shocks moving in opposite direction: top end and bottom end of the plume. Two-dimensional numerical model was used to understand the plume evolution in terms of viscosity ratio and the capillary number. The study found that the buoyancy force causes the

plume to rise up about 500 meter in 700 years. Juanes and MacMinn (2008) proposed a one-dimensional sharp-interface mathematical model for CO_2 migration in saline aquifers. The model accounted for the capillary trapping and gravity override. The CO_2 plume shape was different from previous researches in that the flow of regional groundwater was taken into account. The buoyancy forces lead to gravity override while capillary trapping delays the development of override. Three dimensionless groups: the mobility ratio between CO_2 and water, the gravity number, and trapping coefficient are the key factors that influent shape of CO_2 plume. The capillary trapping coefficient was upscaled from laboratory scale to the basin scale through a formulation based on analytical solution to the model. Nghiem et al. (2009) examined the two most important trapping mechanism for CO_2 storage in saline aquifers: residual gas trapping and solubility trapping. Their study compared how a water injector that is above a CO_2 injector affects the storage of CO_2. In other words, the formation that is used to store CO_2 lies below the saline aquifer. The results indicated that the low permeability aquifer above the CO_2-storage formation can increase the storage capacity while high permeability one does not increase CO_2 trapping. Oloruntobi and LaForce (2009) conducted experimental study to investigate the effect of heterogeneity on buoyancy-driven flow in CO_2 storage. Air was used in the study. The study focused on post-injection period when the migration of CO_2 plume in an aquifer is mainly due to the buoyancy drive that results from the density contrast between the injected CO_2 and formation brine. The study showed that air migration through a homogeneous sand pack provided a more uniform front than the heterogeneous sand pack. A high permeability streak in the sand pack reduced the trapping capacity of the entire pack. The presence of a low-permeability layer in the sand pack increased its trapping capacity. The results also depicted that better consolidated sands trapped more air than poorly consolidated sands. Mantilla et al. (2009) used injection data to assess the migration of plume through adapting a probabilistic history matching software originally developed for oil field applications. The software assimilates injection data commonly monitored at active and inactive wells into models for the subsurface aquifer/reservoir. The algorithm yields an ensemble of realizations geologically consistent with the initial model such that the uncertainty in CO_2 plume location can be easily assessed. The updated models obtained after the history matching process detected the presence of the streak, and the subsequent estimation of CO_2 plume location was much more accurate. Murray et al. (2010) summarized a CO_2 sequestration monitoring in a low formation water salinity reservoir in Japan. The targeted reservoir's water salinity is not sufficiently saline so that uncertainty in the Sigma logging approach increases. To overcome this apparent complication, Sigma logging and alternative measurements such as inelastic ratios and neutron porosity were acquired and combined with the open-hole resistivity, neutron-density and magnetic resonance logs to derive a robust interpretation. Liner et al. (2011) used simulation model to evaluate CO_2 sequestration potential in a deep saline aquifer system in Ness County, Kansas. The study showed that a careful simulation study can maximize CO_2 injection rate, minimize existence of free CO_2, and significantly reduce uncertainty in the safety of CO_2 permanent storage. Amirlatifi et al. (2012) studied the storage of CO_2 in a generic anticline structure. The influence of layer thickness, wavelength and amplitudes at different depths and under different boundary conditions on the maximum CO_2 storage amount was investigated. Their 3-dimensional model was created by finite element analysis preprocessor. Fluid flow under different geometrical and physical conditions was simulated. Pilisi et al. (2012) investigated the technical feasibility of CO_2 sequestration in deepwater offshore Japan. Sub-seabed formations at water depth of 9000 ft in three sites are selected to conduct reservoir simulation. The study indicated that CO_2 capturing technologies and transportation means are at mature stage and drilling vessels are capable to drill well in such deep water. From the technical point of view, CO_2 sequestration in sub-seabed geological formation is feasible. The three studied sites are appropriate for CO_2 storage. Adebayo et al. (2014) emphasized the importance of CO_2 saturation in aquifer during the sequestration. They determined Archie's saturation exponent for CO_2 sequestration in carbonate reservoirs. They proposed a method that can capture the effect of CO_2/brine/rock interaction. The method was compared with conventional porous plate method

and it was found that the saturation index differs for both methods largely due to change in pore geometry during CO_2 storage. Park et al. (2015) analyzed the influence of heterogeneous capillary pressure on CO_2 sequestration under different wetting conditions. In their study, numerical simulations are used to estimate the quantity of CO_2 trapped by dissolution, residual, and capillary trapping. Sensitivity analysis is implemented regarding heterogeneity and CO_2/brine wettability. The research depicted that CO_2 leakage decreases as the permeability variation increases. In strongly water-wet system, the largest portion of stored CO_2 is immobilized. Ajibola et al. (2016) believed the dominant mixing mechanism is convective mixing rather than pure diffusion is important as this controls the timescale over which the carbon dioxide-saturated brine mixes with the unsaturated brine. They used a finite difference reservoir simulator to evaluate the predictions of analytical solutions for stability analysis and growth rate of the fingers of different wavenumbers at different Rayleigh numbers. The effects of density difference, permeability anisotropy and diffusion on fingering behavior were investigated through the dimensionless Rayleigh number. The density difference and the vertical permeability were found to mainly control the degree of instability. Ratnakar et al. (2018) predicted gas solubility in brine solutions for CO_2 capture and sequestration. They extended the Setschenow approach by expressing the solubility in terms of ionic strengths and molar concentrations of each salt. The method also characterized each component (gas, anions and cations) against the experimental measurements. A simple methodology was proposed to predict the impact of types of salts on solubility of CO_2.

In the CO_2 sequestration process, the injected CO_2 is displacing water from the injection point and is expected to remain in the reservoir. Due to the nature of one phase displacing another phase in porous media, it is noted that different water saturation exists in the CO_2 plume during the displacement. Water distribution in the plume will affect the size of the plume subsurface. Furthermore, the gravitational segregation between CO_2 and water will cause overriding- tonguing during the injection and impact the shape of plume. To better understand the CO_2 movement underground and development of CO_2 plume, it is necessary to take the two-phase flow and gravity force effects into account when evaluating CO_2 displacing water. The purpose of this study is to develop a simple and practical model to predict the evolution of the shape of CO_2 plume in the injection and post-injection period.

Model Development

The displacement of water by injecting CO_2 is not a piston-like process in aquifer. Because water is the wetting phase and CO_2 is the non-wetting phase when two phases flow in reservoir, water occupies the surface of matrix and small pores while CO2 resides in large pores and centers of pores. As CO_2 is injected into aquifer, CO_2 displaces water away from the injector through the fractional flow. At the same time, CO_2 migrates upward due to the buoyancy forces. As a result, in the horizontal direction, CO_2 migration is controlled by relative permeability and capillary pressure. Meanwhile, in the vertical direction, the upward migration of CO_2 is affected by relative permeability, capillary pressure and buoyancy force.

Figure 3 shows a circular aquifer with an injector located in the center. For CO_2 sequestration in aquifer, Figure 3 can represent the sequestration procedure well. The fractional flow can be viewed as CO_2 displacing water away from the injector. Figure 4 illustrates the flow line and pressure distribution in the reservoir. To make the analysis simple, following assumptions are made:

1) A circular aquifer with constant height
2) Reservoir is homogenous in all rock properties
3) The dip angle of formation is zero

4) CO_2 and water two-phase flow in reservoir
5) Compressibility of water is negligible
6) The variation in water densities can be neglected
7) Reservoir temperature is constant
8) All rock properties do not change during the sequestration.
9) Constant water viscosities during the displacement
10) Average values are used for CO_2 properties such as viscosity, z-factor, and density when CO_2 flows in reservoir
11) Chemical reaction or the dissolution/precipitation can be ignored.

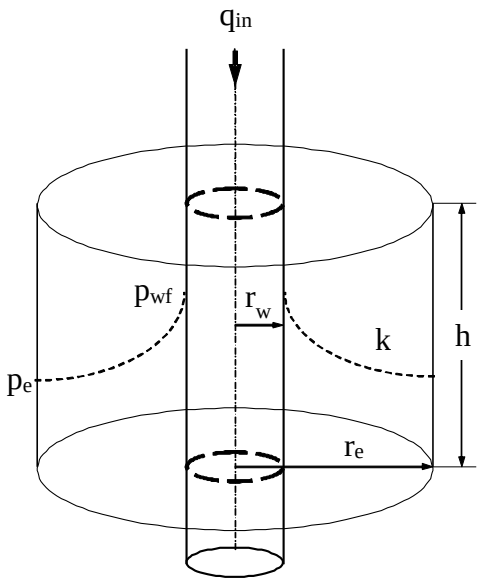

Figure 3. A circular aquifer with an injector located in the center

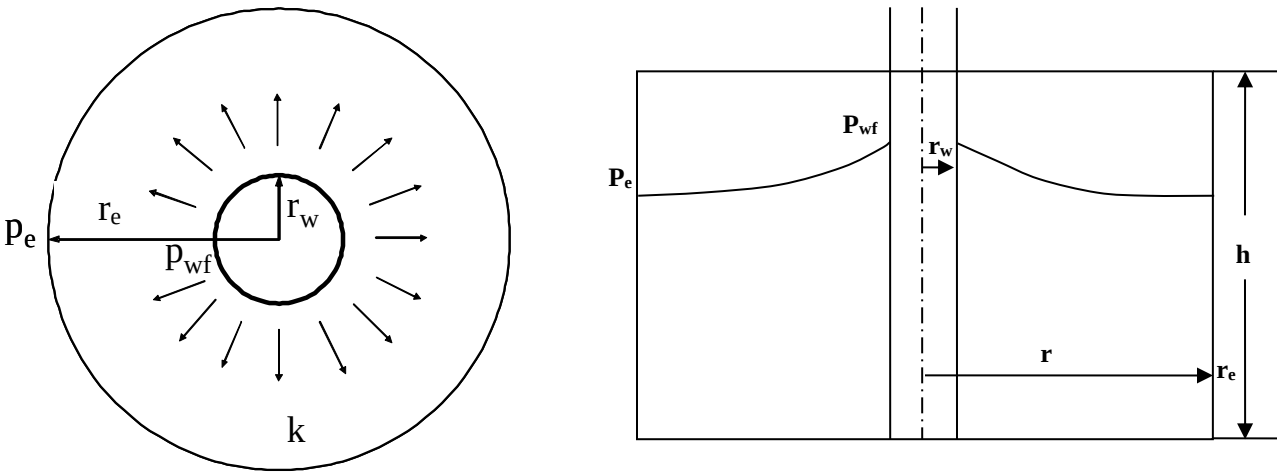

Figure 4. Reservoir system for CO_2 displacing water away from injector: (left) plan view, (right) lateral view

The flow occurs in two directions: horizontal and vertical flows. We first derive the two-phase flow in horizontal direction. Then vertical flow, or segregation of CO_2 and water in the vertical direction, will be discussed next. In the horizontal direction, CO_2 is displacing water away from the injector. Darcy´s equation gives CO_2 (noted as gas in the derivation) and water flow rates

$$q_g = \frac{kk_{rg}}{\mu_g}\frac{\partial(Ap_g)}{\partial r} \quad (1)$$

$$q_w = \frac{kk_{rw}}{\mu_w}\frac{\partial(Ap_w)}{\partial r} \quad (2)$$

where

A= flow area

k = reservoir permeability

k_{rg} = relative permeability to gas

k_{rw} = relative permeability to water

p_g = gas pressure

p_w = water pressure

q_g = gas rate

q_w = water rate

r = radius from wellbore

μ_g = gas viscosity

μ_w = water viscosity

In the displacement, CO_2 is the non-wetting phase and water is the wetting phase. Recalling the concept of capillary pressure, we have

$$P_c = p_g - p_w \quad (3)$$

where

P_c = capillary pressure

Replacing water pressure by gas and capillary pressure **Equation** (2) becomes

$$q_w = \frac{kk_{rw}}{\mu_w}\frac{\partial[A(p_g - p_c)]}{\partial r} \quad (4)$$

Expressing in pressure gradient, **Equations** (1) and (4) are changed to

$$\frac{\partial(Ap_g)}{\partial r} = \frac{\mu_g}{kk_{rg}}q_g \quad (5)$$

$$\frac{\partial(Ap_g)}{\partial r} - \frac{\partial(AP_c)}{\partial r} = \frac{\mu_w}{kk_{rw}}q_w \quad (6)$$

Subtracting **Equation** (5) from (6) we obtain

$$-\frac{\partial(AP_c)}{\partial r} = \frac{\mu_w}{kk_{rw}}q_w - \frac{\mu_g}{kk_{rg}}q_g$$

or

$$\frac{\partial(AP_c)}{\partial r} = \frac{1}{k}\left(\frac{\mu_g}{k_{rg}}q_g - \frac{\mu_w}{k_{rw}}q_w\right) \quad (7)$$

At this stage we can introduce the concepts of total fluid rate and fractional flow, which are defined as

$$q_t = q_g + q_w \quad (8)$$

$$f_g = \frac{q_g}{q_t} \text{ and } f_w = \frac{q_w}{q_t} \quad (9)$$

where

q_t = total fluid rate

f_g = gas fraction

f_w = water fraction

Substituting **Equations** (8) and (9) into (7) yields

$$f_g = \frac{1+\frac{\partial(AP_C)kk_{rw}}{\partial r \quad q_t\mu_w}}{1+\frac{k_{rw}\mu_g}{k_{rg}\mu_w}} \quad \text{..... (10)}$$

Flow area is defined as

$$A = 2\pi rh \quad \text{..... (11)}$$

where

h = reservoir thickness

Substituting **Equation** (11) into (10) we have

$$f_g = \frac{1+\frac{2\pi hkk_{rw}}{q_t\mu_w}\left(\frac{r\partial P_c}{\partial r}+P_c\right)}{1+\frac{k_{rw}\mu_g}{k_{rg}\mu_w}} \quad \text{..... (12)}$$

where

$$\frac{\partial P_c}{\partial r} = \frac{\partial P_c}{\partial S_g}\frac{\partial S_g}{\partial r} \quad \text{..... (13)}$$

It should be noted that capillary pressure decreases as radius increases in this case. Therefore $\frac{\partial P_c}{\partial r}$ is negative. If capillary pressure is negligible, **Equation** (12) is simplified to

$$f_g = \frac{1}{1+\frac{k_{rw}\mu_g}{k_{rg}\mu_w}} \quad \text{..... (14)}$$

According to Brooks-Corey (1954 and 1964) capillary pressure model, drainage capillary pressure in the CO_2 sequestration in aquifer can be expressed as

$$P_c = P_d\left(\frac{S_w - S_{wirr}}{1-S_{wirr}}\right)^{\frac{-1}{\lambda}} \quad \text{..... (15)}$$

where

S_{wirr} = the irreducible water saturation

P_d = the threshold pressure.

Brooks and Corey (1954 and 1964) related the parameter λ to the distribution of pore sizes. For narrow distributions, λ is greater than 2; for wide distributions, λ is less than 2. **Equation** (12) indicates that gas fraction is a function of location and injection volume (or injection time if injection rate is kept constant). Now we derive the continuity equation of radial fractional flow. Considering the CO_2 displacing water, material balance equation provides that the mass change in a control volume for a time period can be shown as **Figure** 5. Since the flow direction is from injector to aquifer outer boundary, we define the center of wellbore as the start point, where r=0, and aquifer outer boundary as the end point where r=r_e. Therefore, in the dimensionless analysis, dimensionless radius can be defined as, r_D=r/r_e, the start point has r_D=0, and the end point has r_D=1. Material balance gives

$$\left[\left(q_g\rho_g\right)_r - \left(q_g\rho_g\right)_{r+\Delta r}\right]\Delta t = \pi h[(r+\Delta r)^2 - r^2]\varphi\left[\left(S_g\rho_g\right)^{t+\Delta t} - \left(S_g\rho_g\right)^t\right] \quad \text{..... (16)}$$

where

S_g = gas saturation

ρ_g = gas density

Δt = time period

t = time

Δr= radius incremental

r= radius

r_e= distance between reservoir outer boundary to wellbore

φ = porosity

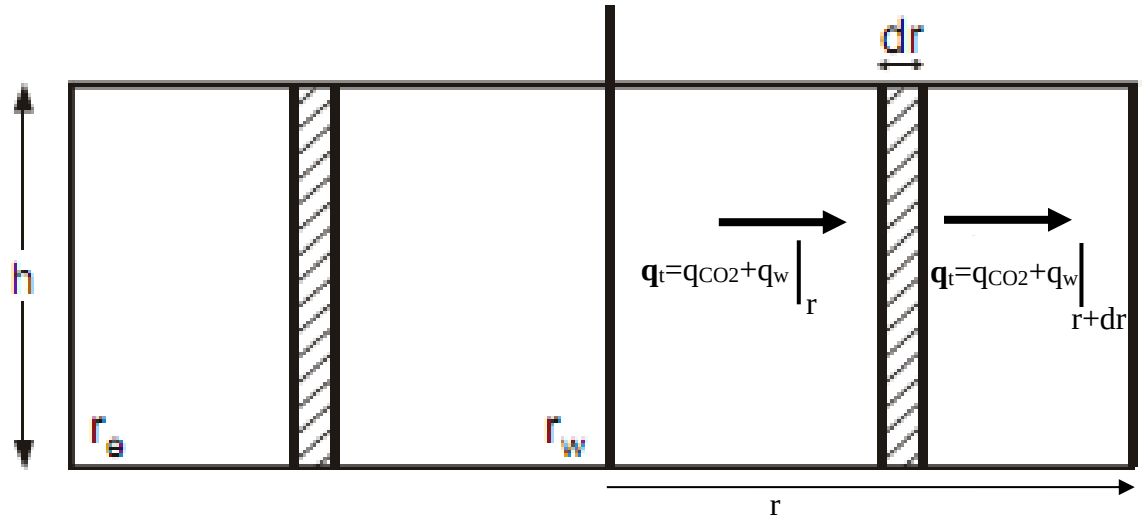

Figure 5. A control volume in a circular aquifer with an injector located in the center.

Simplifying **Equation** (16) we have

$$\left[\left(q_g\rho_g\right)_r-\left(q_g\rho_g\right)_{r+\Delta r}\right]\Delta t=\pi h[2r\Delta r+(\Delta r)^2]\varphi\left[\left(S_g\rho_g\right)^{t+\Delta t}-\left(S_g\rho_g\right)^t\right]. \quad (17)$$

As $\Delta r\to 0$ and $\Delta t\to 0$, we have

$$2r\Delta r+(\Delta r)^2\approx 2r\Delta r. \quad (18)$$

Equation (17) becomes partial differential equation

$$-\frac{\partial(q_g\rho_g)}{\partial r}=2r\pi h\varphi\frac{\partial(S_g\rho_g)}{\partial t}. \quad (19)$$

If an average gas density is used and is assumed constant, we have

$$-\frac{\partial q_g}{\partial r}=2r\pi h\varphi\frac{\partial S_g}{\partial t}. \quad (20)$$

Substituting **Equation** (9) into (20) gives

$$-\frac{\partial(f_g q_t)}{\partial r}=2r\pi h\varphi\frac{\partial S_g}{\partial t}. \quad (21)$$

If CO_2 injection rate is constant and an average CO_2 density at aquifer temperature and average pressure (average of injection pressure and aquifer outer boundary pressure) is used to represent CO_2 density in aquifer, we have a constant total fluid rate. **Equation** (21) can be simplified to

$$-\frac{\partial f_g}{\partial r}=\frac{2r\pi h\varphi}{q_t}\frac{\partial S_g}{\partial t}. \quad (22)$$

Since water fraction is function of water saturation, $f_g(S_g)$, applying chain rule to partial differential equation results in

$$-\frac{df_g}{dS_g}\frac{\partial S_g}{\partial r}=\frac{2r\pi h\varphi}{q_t}\frac{\partial S_g}{\partial t}. \quad (23)$$

Observing that water saturation is function of time, *t*, and position, *r*, we can express

$$dS_g=\frac{\partial S_g}{\partial t}dt+\frac{\partial S_g}{\partial r}dr. \quad (24)$$

The fact that at the displacement front the CO_2 saturation is constant provides us a boundary condition.

$$dS_g=\frac{\partial S_g}{\partial t}dt+\frac{\partial S_g}{\partial r}dr=0$$

or

$$\frac{\partial S_g}{\partial r}=-\frac{\partial S_g}{\partial t}\frac{dt}{dr}. \quad (25)$$

Substituting **Equation** (25) into (23) yields

$$\frac{df_g}{dS_g}dt = \frac{2r\pi h\varphi}{q_t}dr \quad (26)$$

Integrating **Equation** (26) yields an equation for displacement front position, r_f.

$$r_f^2 = \frac{tq_t}{\pi h\varphi}\left(\frac{df_g}{dS_g}\right)_f \quad (27)$$

where

r_f = displacement front position in radial aquifer

There are two solutions to **Equation** (27), which are

$$r_f = \pm\sqrt{\frac{tq_t}{\pi h\varphi}\left(\frac{df_g}{dS_g}\right)_f} \quad (28)$$

Obviously only one solution is correct to match with the physical phenomenon. Considering the fact that location can only be positive, therefore we can eliminate the solution

$$r_f = -\sqrt{\frac{tq_t}{\pi h\varphi}\left(\frac{df_g}{dS_g}\right)_f} \quad (29)$$

Therefore, the correct solution is

$$r_f = \sqrt{\frac{tq_t}{\pi h\varphi}\left(\frac{df_g}{dS_g}\right)_f} \quad (30)$$

For any CO_2 saturation that is behind the displacement front, S_g, the position can be calculated by

$$r_{Sg} = \sqrt{\frac{tq_t}{\pi h\varphi}\left(\frac{df_g}{dS_g}\right)_{Sg}} \quad (31)$$

where

r_{Sg} = position of any CO_2 saturation that is behind the displacement front

Water saturation ahead of the displacement front is the initial water saturation in reservoir. For aquifer, initial water saturation can be assumed 100%. CO_2 saturation ahead of displacement front is 0. Therefore, locations of different CO_2 saturations can be estimated accordingly based on **Equations** (31). **Figure** 7 shows the plot of CO_2 saturation versus radius at different injection times assuming vertical segregation of CO_2 and water can be ignored.

Because of the density difference between CO_2 and water. Segregation between CO_2 and water occurs when CO_2 mixes with water in reservoir. In the segregation, water flows downward while CO_2 flows upward. Considering a control volume around the well (or a ring-shape of reservoir volume) at a radius of r, material balance gives

$$[(q_{wV}\rho_w)_{z+\Delta z} - (q_{wV}\rho_w)_z]\Delta t = A\Delta z\varphi[(S_w\rho_w)^{t+\Delta t} - (S_w\rho_w)^t] \quad (32)$$

where

q_{wV} = water flowrate in vertical direction

ρ_w = water density

A = flow area of control volume when vertical flow occurs

Δz= incremental in vertical direction

S_w = water saturation

As $\Delta z \to 0$ and $\Delta t \to 0$, we have

Equation (32) becomes partial differential equation

$$\frac{\partial(q_{wV}\rho_w)}{\partial z} = A\varphi\frac{\partial(S_w\rho_w)}{\partial t} \quad (33)$$

Assuming constant water density, **Equation (33)** can be simplified to

$$\frac{\partial(q_{wV})}{\partial z} = A\varphi\frac{\partial(S_w)}{\partial t}$$ (34)

The flow of fluid in vertical direction is controlled by buoyancy forces, capillary pressure, and vertical permeability. While the buoyancy force facilitates the water downward migration, the effect of capillary pressure depends on the wettability. In CO_2-water system, water is wetting phase and CO_2 is non-wetting phase. Therefore, capillary pressure facilitates water flow as well. Darcy law gives

$$q_{wV} = A\frac{k_V k_{rw}}{\mu_w}\frac{\Delta z(\rho_w-\rho_g)+P_c}{\Delta z}$$ (35)

where

k_V = vertical permeability

Substituting **Equation (35)** into **(34)** yields

$$\frac{\frac{k_V}{\mu_w}(\rho_w-\rho_g)\partial(k_{rw})}{\partial z} + \frac{\partial\left(\frac{P_c}{\Delta z}\right)}{\partial z} = \varphi\frac{\partial(S_w)}{\partial t}$$ (36)

If capillary pressure is negligible, **Equation (36)** can be simplified to

$$\frac{\frac{k_V}{\mu_w}(\rho_w-\rho_g)\partial(k_{rw})}{\partial z} = \varphi\frac{\partial(S_w)}{\partial t}$$ (37)

Material balance is also applied to CO_2 vertical flow

$$\left[\left(q_{gV}\rho_g\right)_z - \left(q_{gV}\rho_g\right)_{z+\Delta z}\right]\Delta t = A\Delta z\varphi\left[\left(S_g\rho_g\right)^{t+\Delta t} - \left(S_g\rho_g\right)^{t}\right]$$ (38)

where

q_{gV} = gas flowrate in vertical direction

As $\Delta z \to 0$ and $\Delta t \to 0$, we have

Equation (38) becomes partial differential equation

$$-\frac{\partial(q_{gV}\rho_g)}{\partial z} = A\varphi\frac{\partial(S_g\rho_g)}{\partial t}$$ (39)

Assuming average gas density is used, **Equation (39)** can be simplified to

$$-\frac{\partial(q_{gV})}{\partial z} = A\varphi\frac{\partial(S_g)}{\partial t}$$ (40)

Buoyancy force facilitates the gas upward migration while capillary pressure has the opposite effect. Darcy law gives

$$q_{gV} = A\frac{k_V k_{rg}}{\mu_g}\frac{\Delta z(\rho_w-\rho_g)-P_c}{\Delta z}$$ (41)

Substituting **Equation (41)** into **(40)** yields

$$-\frac{\frac{k_V}{\mu_g}(\rho_w-\rho_g)\partial(k_{rg})}{\partial z} + \frac{\partial\left(\frac{P_c}{\Delta z}\right)}{\partial z} = \varphi\frac{\partial(S_g)}{\partial t}$$ (42)

If capillary pressure is negligible, **Equation (42)** can be simplified to

$$-\frac{\frac{k_V}{\mu_g}(\rho_w-\rho_g)\partial(k_{rg})}{\partial z} = \varphi\frac{\partial(S_g)}{\partial t}$$ (43)

Coupling **Equation** (31) for horizontal flow with **Equations (37)** and **(43)** for vertical CO_2-water segregation, CO_2 saturation distribution in the aquifer at different injection times or post-injection periods can be calculated.

Case Study

A case study was conducted to illustrate the analysis of CO_2 displacing water in aquifer. The input data are shown in **Tables** 3. **Table** 4 is the relative permeabilities versus gas and water saturations. Figure 6 shows the capillary pressures of CO_2-water system versus water saturation used in the case study. It is a drainage curve that simulates non-wetting phase (CO_2) displacing water (wetting phase).

Table 3. The input data for CO_2 displacing water in an aquifer system

CO_2 injection rate at standard conditions	=	20,000	Mscf/day
Aquifer radius	=	10,000	ft
Aquifer thickness	=	100	ft
Initial water saturation	=	100%	
Irreducible water saturation	=	20.0%	
Residual CO_2 saturation	=	25.0%	
CO_2 viscosity	=	0.02	cp
Water viscosity	=	1.0	cp
Porosity	=	20.0%	
Reservoir horizontal permeability	=	200	mD
Reservoir vertical permeability	=	20, 100, or 200	mD
Reservoir temperature	=	150	^oF
Average pressure in injection calculation	=	3500	psia
Aquifer porosity	=	0.25	
CO_2 compressibility factor at reservoir conditions	=	1	

Table 4. The relative permeabilities versus water saturation

No.	**Sw**	**Sg**	**krw**	**krg**
	0	1	0	0.5
1	0.2	0.8	0	0.5
2	0.209	0.791	0.0001	0.4838
3	0.218	0.782	0.0005	0.4678
4	0.227	0.773	0.0012	0.4522
5	0.236	0.764	0.0021	0.4368
6	0.245	0.755	0.0033	0.4216
7	0.254	0.746	0.0048	0.4067
8	0.263	0.737	0.0065	0.3921
9	0.272	0.728	0.0085	0.3778
10	0.281	0.719	0.0108	0.3637
11	0.290	0.710	0.0134	0.3499
12	0.299	0.701	0.0162	0.3364
13	0.308	0.692	0.0192	0.3231
14	0.317	0.683	0.0226	0.3101
15	0.326	0.674	0.0262	0.2974
16	0.335	0.665	0.0300	0.2849
17	0.344	0.656	0.0342	0.2727
18	0.353	0.647	0.0386	0.2608

19	0.362	0.638	0.0433	0.2491
20	0.371	0.629	0.0482	0.2377
21	0.380	0.620	0.0534	0.2266
22	0.389	0.611	0.0589	0.2157
23	0.398	0.602	0.0646	0.2051
24	0.407	0.593	0.0706	0.1948
25	0.416	0.584	0.0769	0.1847
26	0.425	0.575	0.0835	0.1749
27	0.434	0.566	0.0903	0.1654
28	0.443	0.557	0.0974	0.1561
29	0.452	0.548	0.1047	0.1471
30	0.461	0.539	0.1123	0.1384
31	0.470	0.530	0.1202	0.1299
32	0.479	0.521	0.1283	0.1217
33	0.488	0.512	0.1368	0.1138
34	0.497	0.503	0.1454	0.1061
35	0.506	0.494	0.1544	0.0987
36	0.515	0.485	0.1636	0.0916
37	0.524	0.476	0.1731	0.0847
38	0.533	0.467	0.1828	0.0781
39	0.542	0.458	0.1928	0.0718
40	0.551	0.449	0.2031	0.0657
41	0.560	0.440	0.2137	0.0600
42	0.569	0.431	0.2245	0.0544
43	0.578	0.422	0.2356	0.0492
44	0.587	0.413	0.2469	0.0442
45	0.596	0.404	0.2586	0.0395
46	0.604	0.396	0.2704	0.0350
47	0.613	0.387	0.2826	0.0308
48	0.622	0.378	0.2950	0.0269
49	0.631	0.369	0.3077	0.0232
50	0.640	0.360	0.3207	0.0198
51	0.649	0.351	0.3339	0.0167
52	0.658	0.342	0.3474	0.0139
53	0.667	0.333	0.3611	0.0113
54	0.676	0.324	0.3751	0.0090
55	0.685	0.315	0.3894	0.0069
56	0.694	0.306	0.4040	0.0051
57	0.703	0.297	0.4188	0.0036
58	0.712	0.288	0.4339	0.0023
59	0.721	0.279	0.4493	0.0014
60	0.730	0.270	0.4649	0.0006

61	0.739	0.261	0.4808	0.0002
62	0.748	0.252	0.4969	0.0000
63	0.757	0.243	0.5000	0.0000
64	0.766	0.234	0.5000	0.0000
65	0.775	0.225	0.5000	0.0000
66	0.784	0.216	0.5000	0.0000
67	0.793	0.207	0.5000	0.0000
68	0.802	0.198	0.5000	0.0000
69	0.811	0.189	0.5000	0.0000
70	0.820	0.180	0.5000	0.0000
71	0.829	0.171	0.5000	0.0000
72	0.838	0.162	0.5000	0.0000
73	0.847	0.153	0.5000	0.0000
74	0.856	0.144	0.5000	0.0000
75	0.865	0.135	0.5000	0.0000
76	0.874	0.126	0.5000	0.0000
77	0.883	0.117	0.5000	0.0000
78	0.892	0.108	0.5000	0.0000
79	0.901	0.099	0.5000	0.0000
80	0.910	0.090	0.5000	0.0000
81	0.919	0.081	0.5000	0.0000
82	0.928	0.072	0.5000	0.0000
83	0.937	0.063	0.5000	0.0000
84	0.946	0.054	0.5000	0.0000
85	0.955	0.045	0.5000	0.0000
86	0.964	0.036	0.5000	0.0000
87	0.973	0.027	0.5000	0.0000
88	0.982	0.018	0.5000	0.0000
89	0.991	0.009	0.5000	0.0000
90	1.000	0.000	0.5000	0.0000

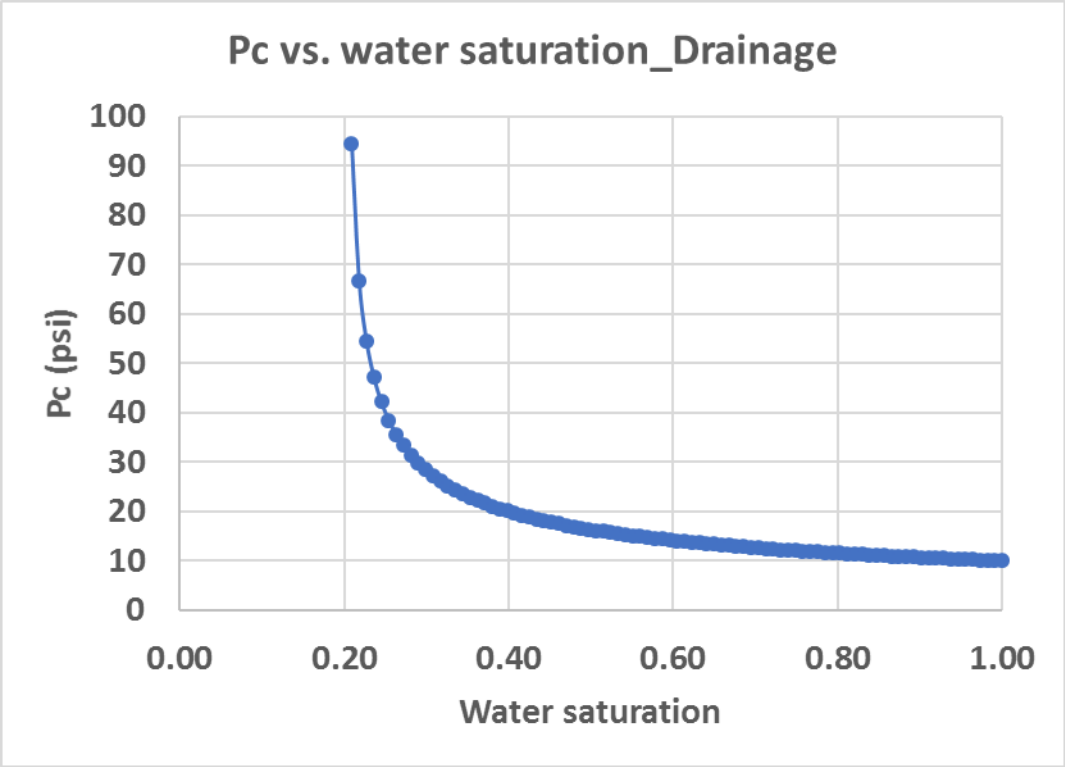

Figure 6. Capillary pressure versus water saturation for the CO_2 displacing water in aquifer during injection

If vertical segregation is ignored, CO_2 saturation at any radius is a unique number and is constant at different aquifer elevations. **Figure 7** illustrates the CO_2 saturation distribution along the radius of aquifer at different injection times. In this case, CO_2 saturation at the displacement front is 0.342. Ahead of the displacement front, water saturation is 100%, or CO_2 saturation is 0.0%. The location of displacement front at different injection time can be found in **Table 5**. **Figure 7** and **Table 5** indicate that movement of CO_2 saturation away from the well is not linear to the injection time. The movement slows down because more pore volumes needed to be filled as radius increases.

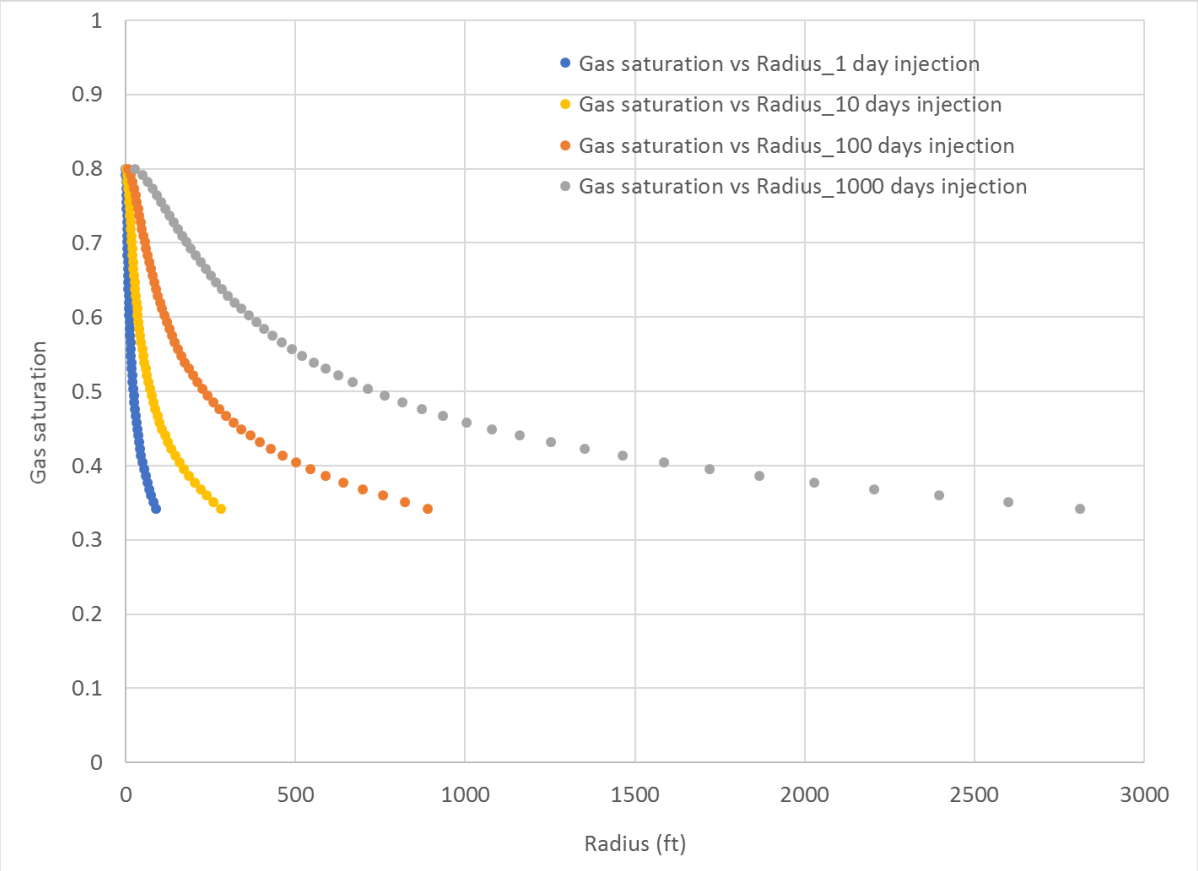

Figure 7. Change of CO_2 saturation in aquifer during different injection times

Table 5. Location of displacement front at different injection times

Injection time (days)	1	2	5	10	20	50	100	200	500	1000	2000	5000	10000
Displacement front Location (ft)	89	126	199	281	398	629	889	1257	1988	2811	3976	6286	8890

CO_2-water segregation causes CO_2 to migrate to the top of aquifer. **Figure 8** depicts the variation of CO_2 saturation from the bottom of aquifer to the top of aquifer at different radii. It can be seen that near the wellbore the segregation is more complete than away from the wellbore, which is indicated by wide ranges of CO_2 saturation between the bottom of aquifer (with aquifer elevation of 0 ft) and the top of aquifer (with aquifer elevation of 100 ft). The segregation leads to the overriding of CO_2 on water during the injection and for post-injection period. Increasing injection rate can reduce the overriding effect temporary, but segregation will occur until the buoyancy force is balanced by the capillary force. At the beginning of the segregation, the difference between the buoyancy force and capillary force is the highest. The force difference that causes the CO_2 vertical-migration is the largest. As gas migration continues, capillary force increases. Therefore, the segregation speed is highest at the beginning and then slows down as time goes on. Once the buoyancy force is equal to capillary force, CO_2-water system reaches a dynamic equilibrium status and CO_2 will remain in location until the equilibrium is broken.

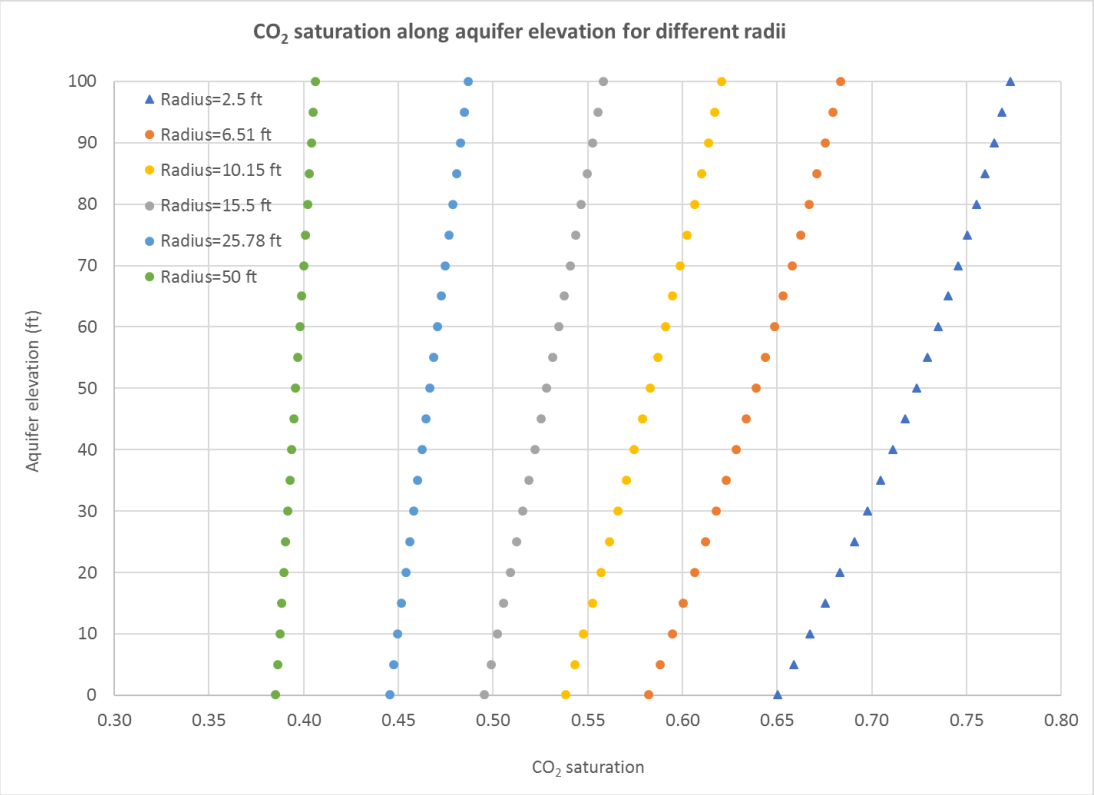

Figure 8. Change of CO_2 saturation along aquifer elevation at different radii

Anisotropy of rock properties is often observed in aquifer. For most aquifers vertical permeability is less than horizontal permeability, which alleviates the CO_2 vertical migration. In this study, the effect of vertical/horizontal permeability ratio on the CO_2 overriding on water is investigated. Three cases with vertical/horizontal permeability ratio of 1.0, 0.5 and 0.1 are compared to analyze how low vertical permeability delays the CO_2 upward migration. One should note that low permeability also means high capillary pressure, which also limits the upward flow of CO_2. **Figure 9** shows the CO_2 saturation distribution along aquifer elevation for different vertical/horizontal permeability ratios at two radii. It clearly shows that low vertical/horizontal permeability ratio has less CO_2 overriding than that of high vertical/horizontal permeability ratio.

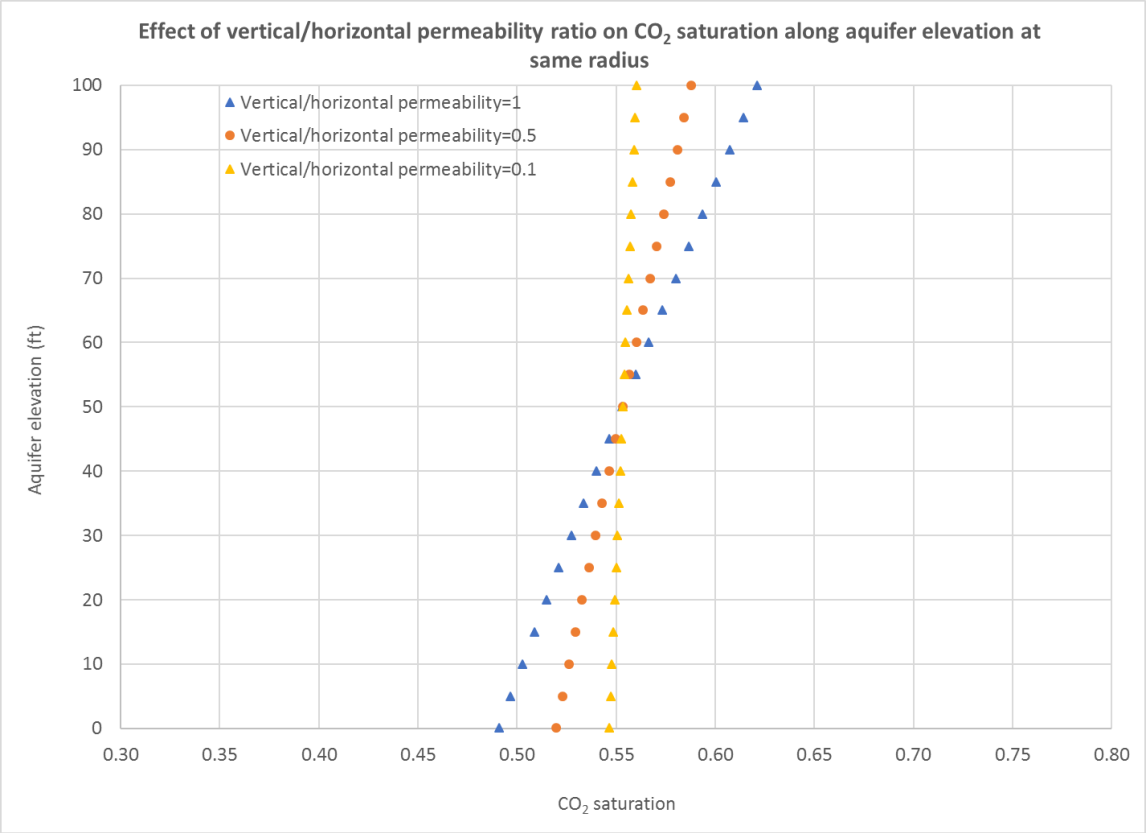

Figure 9. Effect of permeability anisotropy on CO_2-water segregation at same radius

Conclusions

Following conclusions can be drawn upon this study.

- A model coupling CO_2-water fractional flow in horizontal direction with CO2-water segregation in vertical direction has been proposed. It can be used to simulate the performance of CO_2 sequestration in aquifer.
- The model indicates that CO_2 displacing water is not a piston-like displacement. CO_2 saturation at the displacement front is a function of fluid and rock properties. Behind the CO_2 front, CO_2 saturation increases gradually, and water saturation decreases accordingly until water saturation reaches irreducible water saturation.
- The propagation of CO_2 front is not linear to the injection time. Its movement slows down as it moves away from injection well.
- For same radius, CO_2-water segregation causes higher CO_2 saturation at top of aquifer and low at the bottom of aquifer.
- Low vertical/horizontal permeability ratio can delay CO_2-water segregation, leads to a less severity of CO_2 overriding.

Acknowledgement

The authors are grateful to The Petroleum Engineering Department at the University of North Dakota. This research is supported in part by the North Dakota EPSCoR Program under award number EPS-0814442 and by Peng Yu: Guangxi Natural Science Foundation (No.2016GXNSFBA380180 and No. 2017GXNSFAA198105).

Nomenclature

A= flow area
A = flow area of control volume when vertical flow occurs
f_g = gas fraction
f_w = water fraction
h = reservoir thickness
k = reservoir permeability
k_{rg} = relative permeability to gas
k_{rw} = relative permeability to water
k_V = vertical permeability
P_c = capillary pressure
P_d = the threshold pressure.
p_g = gas pressure
p_w = water pressure
q_g = gas rate
q_{gV} = gas flowrate in vertical direction
q_t = total fluid rate
q_w = water rate
q_{wV} = water flowrate in vertical direction
r = radius from wellbore
r_e = distance between reservoir outer boundary to wellbore
r_f = displacement front position in radial aquifer
r_{Sg} = position of any CO_2 saturation that is behind the displacement front
S_g = gas saturation
S_w = water saturation
S_{wirr} = irreducible water saturation
t = time
μ_g = gas viscosity
μ_w = water viscosity
ρ_g = gas density
ρ_w = water density
φ = porosity
Δt = time period
Δr= radius incremental
Δz= incremental in vertical direction

References

1. Adebayo, A. R., Al-Yousef, H. Y., & Mahmoud, M. (2014, August 5), "Determination of Archie's Saturation Exponent for CO_2 Sequestration in Carbonate Reservoirs", *Society of Petroleum Engineers*, doi:10.2118/172354-MS.
2. Ajibola, J., Adam, A., & Muggeridge, A. (2016, October 25), "Gravity Driven Fingering and Mixing During CO_2 Sequestration", *Society of Petroleum Engineers*, doi:10.2118/182317-MS.
3. Amirlatifi, A., Eckert, A., Nygaard, R., Bai, B., Liu, X., & Paradeis, M. (2012, January 1), "Role of Geometrical Influences of CO_2 Sequestration in Anticlines", *American Rock Mechanics Association*.
4. Bennion, B., & Bachu, S. (2005, January 1), "Relative Permeability Characteristics for Supercritical CO_2 Displacing Water in a Variety of Potential Sequestration Zones", *Society of Petroleum Engineers*, doi:10.2118/95547-MS.
5. Brooks, R.H. and Corey, A.T. (1964), "Hydraulic properties of porous media", *Hydrology Paper No. 3*, Colorado State University, Fort Collins, Colorado, 22–27.
6. Corey, A.T. (1954), "The interrelation between gas and oil relative permeabilities", *Producers Monthly* 19 (November): 38–41.
7. Frailey, S. M. (2004, January 1), "Material Balance Reservoir Model for CO_2 Sequestration in Depleted Gas Reservoirs", *Society of Petroleum Engineers*, doi:10.2118/90669-MS.
8. Hannah Ritchie and Max Roser (2019), "CO_2 and other Greenhouse Gas Emissions", Published online at *OurWorldInData.org*, Retrieved from https://ourworldindata.org/co2-and-other-greenhouse-gas-emissions.
9. Haynes, H. M., ed. (2016), *CRC Handbook of Chemistry and Physics*(97th ed.), CRC Press, p. 14-3, ISBN 978-1-4987-5428-6.
10. House, N. J., Faulder, D. D., Olson, G. L., & Fanchi, J. R. (2003, January 1), "Simulation Study of CO_2 Sequestration in a North Sea Formation. Society of Petroleum Engineers", doi:10.2118/81202-MS.
11. Izgec, O., Demiral, B., Bertin, H. J., & Akin, S. (2005, January 1), "Experimental and Numerical Investigation of Carbon Sequestration in Saline Aquifers", *Society of Petroleum Engineers*, doi:10.2118/94697-STU.
12. Juanes, R., & MacMinn, C. (2008, January 1), "Upscaling of Capillary Trapping Under Gravity Override: Application to CO_2 Sequestration in Aquifers", Society of Petroleum Engineers. doi:10.2118/113496-MS.
13. Liner, C., Geng, P., Zeng, J., King, H., & Li, J. (2011, January 1), "A CO_2 Sequestration Simulation Case Study at the Dickman Field", Ness Co., Kansas. Society of Petroleum Engineers, doi:10.2118/145791-MS.
14. Mantilla, C. A., Srinivasan, S., Cross III, E. A., & Bryant, S. L. (2009, January 1), "Inexpensive Assessment of Plume Migration during CO_2 Sequestration", *Society of Petroleum Engineers*, doi:10.2118/126693-MS.
15. Murray, D. R., Yang, X., Horie, T., Yoshimura, T., & Mito, S. (2010, January 1), "CO_2 Sequestration Monitoring in a Low Salinity Reservoir", *Society of Petroleum Engineers*, doi:10.2118/130773-MS.
16. Nghiem, L. X., Yang, C., Shrivastava, V. K., Kohse, B. F., Hassam, M. S., Chen, D., & Card, C. (2009, January 1), "Optimization of Residual Gas and Solubility Trapping for CO_2 Sequestration in Saline Aquifers", *Society of Petroleum Engineers*, doi:10.2118/119080-MS.
17. Oloruntobi, O. S., & LaForce, T. C. (2009, January 1), "Effect of Aquifer Heterogeneity on CO_2 Sequestration", *Society of Petroleum Engineers*, doi:10.2118/121776-MS.

18. Park, S., J., Kim, T. H., & Lee, K. S. (2015, July 27), "Influence of Heterogeneous Capillary Pressure on CO_2 Sequestration in Different Wetting Conditions", *International Society of Offshore and Polar Engineers*.
19. Pilisi, N., Ghorbani, D., & Vasantharajan, S. (2012, January 1), "CO_2 Sequestration in Deepwater Sediments Offshore Japan", *Carbon Management Technology Conference*, doi:10.7122/151756-MS.
20. Ratnakar, R. R., Venkatraman, A., Kalra, A., & Dindoruk, B. (2018, September 24), "On the Prediction of Gas Solubility in Brine Solutions for Applications of CO_2 Capture and Sequestration", *Society of Petroleum Engineers*, doi:10.2118/191541-MS.
21. Riaz, A., & Tchelepi, H. A. (2006, January 1), "Unstable Dynamics of Vertical Displacement in Porous Media Associated With CO_2 Sequestration", *Society of Petroleum Engineers*, doi:10.2118/103169-MS.
22. Sakurai, S., Ramakrishnan, T. S., Boyd, A., Mueller, N., & Hovorka, S. (2006, December 1), "Monitoring Saturation Changes for CO_2 Sequestration: Petrophysical Support of the Frio Brine Pilot Experiment", *Society of Petrophysicists and Well-Log Analysts*.
23. Schembre-McCabe, J. M., Kamath, J., & Gurton, R. M. (2007, January 1), "Mechanistic Studies of CO_2 Sequestration", *International Petroleum Technology Conference*, doi:10.2523/IPTC-11391-MS.
24. Spiteri, E., Juanes, R., Blunt, M. J., & Orr, F. M. (2005, January 1), "Relative-Permeability Hysteresis: Trapping Models and Application to Geological CO_2 Sequestration", *Society of Petroleum Engineers*, doi:10.2118/96448-MS.
25. U.S. EPA, (2019), https://web.archive.org/web/20041112075806/http://www.epa.gov/nonco2/econ-inv/table.html. Retrieved in June 2019.
26. Wallace, John M. and Peter V. Hobbs. (2006), "Atmospheric Science: An Introductory Survey", *Elsevier*, Second Edition, ISBN 978-0-12-732951-2, Chapter 1.